Dynamic dipole polarizabilities of the Li atom and the Be$^+$ ion

Li-Yan Tang,[1,2] Zong-Chao Yan,[3,4,5] Ting-Yun Shi,[1] and J. Mitroy[6]

[1]*State Key Laboratory of Magnetic Resonance and Atomic and Molecular Physics, Wuhan Institute of Physics and Mathematics,*
Chinese Academy of Sciences, Wuhan 430071, People's Republic of China
[2]*Graduate School of the Chinese Academy of Sciences, Beijing 100049, People's Republic of China*
[3]*Center for Cold Atom Physics, Chinese Academy of Sciences, Wuhan 430071, People's Republic of China*
[4]*Department of Physics, Wuhan University, Wuhan 430072, People's Republic of China*
[5]*Department of Physics, University of New Brunswick, Fredericton, New Brunswick, E3B 5A3, Canada*
[6]*School of Engineering, Charles Darwin University, Darwin NT 0909, Australia*

The dynamic dipole polarizabilities for Li atoms and Be$^+$ ions in the $2\,^2S$ and $2\,^2P$ states are calculated using the variational method with a Hylleraas basis. The present polarizabilities represent the definitive values in the nonrelativistic limit. Corrections due to relativistic effects are also estimated. Analytic representations of the polarizabilities for frequency ranges encompassing the $n = 3$ excitations are presented. The recommended polarizabilities for ^{7}Li and ^{9}Be$^+$ are 164.11 ± 0.03 a_0^3 and 24.489 ± 0.004 a_0^3, respectively.

I. INTRODUCTION

The advent of cold-atom physics has lead to increased importance being given to the precise determination of atomic polarizabilities and related quantities. One very important source of systematic error in the new generation of atomic frequency standards is the blackbody radiation (BBR) shift [1–3]. The differential Stark shifts caused by the ambient electromagnetic field leads to a temperature-dependent shift in the transition frequency of the two states involved in the clock transition. The dynamic polarizability is also useful in the determination of the magic wavelength in optical lattices [4–7]. Another area where polarization phenomena is important is in the determination of global potential surfaces for diatomic molecules [8].

When consideration is given to all the atoms and ions commonly used in cold-atom physics, the Li atom and the Be$^+$ ion have the advantage that they have only three electrons. This makes them accessible to calculations using correlated basis sets with the consequence that many properties of these systems can be computed to a high degree of precision. The results of these first-principles calculations can serve as atomic-based standards for quantities that are not amenable to precision measurement. For example, cold-atom interferometry has been used to measure the ground-state polarizabilities of Li and Na atoms [9,10]. However, the polarizability ratio $\alpha_d(X)/\alpha_d(\text{Li})$ can be measured to a higher degree of precision than individual polarizabilities [11]. Thus, measurements of this ratio, in conjunction with a high-precision *ab initio* calculation, could lead to a new level of accuracy in polarizability measurements for the atomic species most commonly used in cold-atom physics.

Calculations and measurements of Stark shifts are particularly important in atomic-clock research since the BBR shift is predominantly determined by the Stark shift of the two levels involved in the clock transition. The best experimental measurements of the Stark shift have been carried out for the alkali-metal atoms, and accuracies better than 0.1% have been reported [12,13]. Experimental work at this level of accuracy relies on a very precise determination of the electric field strength in the interaction region [13–15]. High-precision Hylleraas calculations of the type presented herein provide an invaluable test of the experimental reliability since they provide an independent means for the calibration of electric fields [16].

The dynamic Stark shift in oscillating electromagnetic fields is also of interest. The so-called magic wavelength (i.e., the precise wavelength at which the Stark shifts for upper and lower levels of the clock transition are the same) is an important parameter for optical lattices. The present calculation is used to estimate the magic wavelength for the Li $2\,^2S \rightarrow 2\,^2P$ transition. The present calculations of the ac Stark shift potentially provides an atomic-based standard of electromagnetic (EM) field intensity for finite-frequency radiation.

There have been many calculations of the static polarizabilities of the ground and excited states of Li atoms and Be$^+$ ions [17–23]. The most precise calculations on Li and Be$^+$ are the Hylleraas calculations by Tang and collaborators [17,23]. The Hylleraas calculations were nonrelativistic and also included finite-mass effects for Li. Large-scale calculations using fully correlated Hylleraas basis sets can attain a degree of precision not possible for calculations based on orbital basis sets [19,24,25]. There have been many calculations of the dynamic polarizability for Li [20,26–33], but fewer for Be$^+$ [28,32]. The present calculation is by far the most precise calculation of the dynamic polarizability that is based upon a solution of the nonrelativistic Schrödinger equation. And the present dynamic polarizabilities are obtained at real frequencies, which is different from the work of Derevianko *et al.* [27] who calculated the electric-dipole polarizabilities at imaginary frequencies. One particularly noteworthy treatment is the relativistic single-double all-order many-body perturbation-theory calculation (MBPT-SD) by Safronova *et al.* [33]. This calculation is fully relativistic and treats correlation effects to a high level of accuracy, although it does not achieve the same level of precision as the present Hylleraas calculation.

The present work computes the dynamic dipole polarizabilities of the Li atom and the Be$^+$ ion in the $2\,^2S$ and $2\,^2P$ levels using a large variational calculation with a Hylleraas

basis set. This methodology allows for the determination of the computational uncertainty related to the convergence of the basis set. Analytic representations of the dynamic polarizabilities are made so they can subsequently be computed at any frequency. Finally, the difference between the calculated and experimental binding energies is used to estimate the size of the relativistic correction to the polarizability. The final polarizabilities should be regarded as the recommended polarizabilities for comparison with experiment. All quantities given in this work are reported in atomic units except where indicated otherwise.

II. STRUCTURE CALCULATIONS

A. Hamiltonian and Hylleraas coordinates

The Li atom and Be$^+$ ion are four-body Coulomb systems. After separating the center-of-mass coordinates, the nonrelativistic Hamiltonian can be written in the form [36]

$$H_0 = -\sum_{i=1}^{3} \frac{1}{2\mu} \nabla_i^2 - \frac{1}{m_0} \sum_{i>j\geqslant 1}^{3} \nabla_i \cdot \nabla_j$$
$$- \sum_{i=1}^{3} \frac{Z}{r_i} + \sum_{i>j\geqslant 1}^{3} \frac{1}{r_{ij}}, \quad (1)$$

where $r_{ij} = |\mathbf{r}_i - \mathbf{r}_j|$ is the distance between electrons i and j, $\mu = m_0 m_e/(m_0 + m_e)$ is the reduced mass between the electron and the nucleus, and Z is the nuclear charge. In our calculation, the wave functions are expanded in terms of the explicitly correlated basis set in Hylleraas coordinates:

$$\phi(\mathbf{r}_1, \mathbf{r}_2, \mathbf{r}_3) = r_1^{j_1} r_2^{j_2} r_3^{j_3} r_{12}^{j_{12}} r_{23}^{j_{23}} r_{31}^{j_{31}} e^{-\alpha r_1 - \beta r_2 - \gamma r_3}$$
$$\times \mathcal{Y}^{LM_L}_{(\ell_1 \ell_2)\ell_{12}, \ell_3}(\hat{\mathbf{r}}_1, \hat{\mathbf{r}}_2, \hat{\mathbf{r}}_3) \chi(1,2,3), \quad (2)$$

where $\mathcal{Y}^{LM_L}_{(\ell_1 \ell_2)\ell_{12}, \ell_3}$ is the vector-coupled product of spherical harmonics to form an eigenstate of total angular momentum L and component M_L:

$$\mathcal{Y}^{LM_L}_{(\ell_1 \ell_2)\ell_{12}, \ell_3}(\hat{\mathbf{r}}_1, \hat{\mathbf{r}}_2, \hat{\mathbf{r}}_3)$$
$$= \sum_{\text{all } m_i} \langle \ell_1 m_1 \ell_2 m_2 | \ell_{12} m_{12} \rangle \langle \ell_{12} m_{12} \ell_3 m_3 | LM_L \rangle$$
$$\times Y_{\ell_1 m_1}(\hat{\mathbf{r}}_1) Y_{\ell_2 m_2}(\hat{\mathbf{r}}_2) Y_{\ell_3 m_3}(\hat{\mathbf{r}}_3), \quad (3)$$

and $\chi(1,2,3)$ is the three-electron spin-$\frac{1}{2}$ wave function. The variational wave function is a linear combination of antisymmetrized basis functions ϕ. With some truncations to avoid potential numerical linear dependence, all terms in Eq. (2) are included such that

$$j_1 + j_2 + j_3 + j_{12} + j_{23} + j_{31} \leqslant \Omega, \quad (4)$$

where Ω is an integer. The computational details in evaluating the necessary matrix elements of the Hamiltonian may be found in [25]. The nonlinear parameters α, β, and γ in Eq. (2) are optimized using Newton's method.

The convergence for the energies and other expectation values is studied by increasing Ω progressively. The basis sets are essentially the same as two earlier Hylleraas calculations of the static polarizabilities [17,23]. The maximum Ω used in the present calculations is 12. The uncertainty in the final value
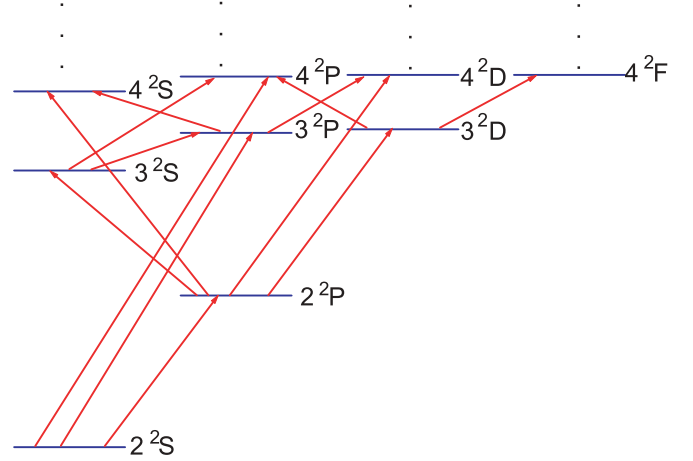

FIG. 1. (Color online) Low-lying energy levels of the Li atom. The energy-level diagram for Be$^+$ is similar.

of any quantity is usually estimated to be equal to the size of the extrapolation from the largest explicit calculation.

Figure 1 is a schematic diagram showing the nonrelativistic energy levels of the most important states of the Li atom. The energy-level diagram for the low-lying states of Be$^+$ is similar.

The energies of the ground states for $^\infty$Li and ^{7}Li are $-7.478\,060\,323\,91(5)$ and $-7.477\,451\,930\,65(5)$ a.u., respectively. The respective energies for the $^\infty$Be$^+$ and ^{9}Be$^+$ ground states are $-14.324\,763\,176\,9(3)$ and $-14.323\,863\,494\,2(3)$ a.u. Table I gives the binding energies of the Li-atom and Be$^+$-ion systems with respect to the two-electron Li$^+$ and Be^{2+} cores. The Hylleraas basis was optimized to compute the $2\,^2S$- and $2\,^2P$-state polarizabilities, so some of the $n = 4$ state energies have significant deviations from the experimental $n = 4$ state energies. The states with significant energy differences can be regarded as pseudostates. The uncertainties listed in Table I represent the uncertainties in energy with respect to an infinite-basis calculation. The actual computational uncertainty is very small and there is no computational error in any of the calculated digits listed in Table I.

With one exception, all the finite-mass binding energies are less tightly bound than experiment. The differences from experiment are most likely due to relativistic effects. The exception where experiment is less tightly bound than the finite-mass calculation is the $4\,^2F$ state of Li. This exception was not investigated since the properties of this state do not enter into any of the polarizability calculations.

B. Polarizability definitions

The dynamic polarizability provides a measure of the reaction of an atom to an external electromagnetic field. The dynamic polarizability at real frequencies can be expressed in terms of a sum over all intermediate states, including the continuum. The dynamic dipole polarizability is expressed in terms of the dynamic scalar and tensor dipole polarizabilities, $\alpha_1(\omega)$ and $\alpha_1^T(\omega)$, which can be expressed in terms of the reduced matrix elements of the dipole transition operator:

$$\alpha_1(\omega) = \sum_{L_a} \alpha_1(L_a, \omega), \quad (5)$$

TABLE I. Comparisons of the binding energies in atomic units (a.u.) of Li and Be^+ in their low-lying states. The experimental valence binding energies are taken from the National Institute of Standards database [34]. The J-weighted average is used for states with $L \geqslant 1$. The ground-state energies for the $^\infty Li^+$ and $^\infty Be^{2+}$ ions are $-7.279\,913\,412\,669\,305\,9$ and $-13.655\,566\,238\,423\,586\,7$ a.u., respectively [35]. The ground-state energies for $^7Li^+$ and $^9Be^{2+}$ are $-7.279\,321\,519\,815\,674\,4$ and $-13.654\,709\,268\,282\,791\,7$ a.u., respectively [35]. Underlining is used to indicate digits that have not converged with respect to basis-set enlargement.

| State | Theory | | Experiment |
	$^\infty Li$	^7Li	$^{6,7}Li$
$2\,^2S$	$-0.198\,146\,911\,\underline{24}$	$-0.198\,130\,410\,\underline{84}$	$-0.198\,142$
$2\,^2P$	$-0.130\,243\,119\,\underline{63}$	$-0.130\,236\,238\,\underline{76}$	$-0.130\,236$
$3\,^2S$	$-0.074\,183\,813\,\underline{50}$	$-0.074\,177\,770\,\underline{25}$	$-0.074\,182$
$3\,^2P$	$-0.057\,237\,698\,\underline{23}$	$-0.057\,234\,245\,\underline{77}$	$-0.057\,236$
$3\,^2D$	$-0.055\,610\,129\,\underline{74}$	$-0.055\,605\,785\,\underline{43}$	$-0.055\,606$
$4\,^2S$	$-0.037\,528\,709\,\underline{57}$	$-0.037\,524\,450\,\underline{73}$	$-0.038\,615$
$4\,^2P$	$-0.031\,390\,736\,\underline{13}$	$-0.031\,388\,143\,\underline{90}$	$-0.031\,975$
$4\,^2D$	$-0.031\,275\,884\,\underline{44}$	$-0.031\,273\,439\,\underline{38}$	$-0.031\,274$
$4\,^2F$	$-0.031\,253\,555\,\underline{31}$	$-0.031\,251\,112\,\underline{02}$	$-0.031\,243$
	$^\infty Be^+$	$^9Be^+$	$^9Be^+$
$2\,^2S$	$-0.669\,196\,938\,\underline{47}$	$-0.669\,154\,225\,\underline{99}$	$-0.669\,247$
$2\,^2P$	$-0.523\,767\,053\,\underline{52}$	$-0.523\,750\,653\,\underline{65}$	$-0.523\,769$
$3\,^2S$	$-0.267\,205\,491\,\underline{76}$	$-0.267\,188\,673\,\underline{34}$	$-0.267\,233$
$3\,^2P$	$-0.229\,567\,886\,\underline{15}$	$-0.229\,558\,220\,\underline{05}$	$-0.229\,582$
$3\,^2D$	$-0.222\,487\,819\,\underline{72}$	$-0.222\,474\,290\,\underline{85}$	$-0.222\,478$
$4\,^2S$	$-0.136\,294\,878\,\underline{43}$	$-0.136\,280\,823\,\underline{70}$	$-0.143\,152$
$4\,^2P$	$-0.122\,229\,244\,\underline{51}$	$-0.122\,219\,998\,\underline{23}$	$-0.128\,134$
$4\,^2D$	$-0.125\,126\,888\,\underline{79}$	$-0.125\,119\,269\,\underline{08}$	$-0.125\,124$
$4\,^2F$	$-0.125\,015\,467\,\underline{11}$	$-0.125\,007\,857\,\underline{69}$	$-0.125\,008$

$$\alpha_1^T(\omega) = \sum_{L_a} W(L,L_a)\alpha_1(L_a,\omega), \qquad (6)$$

where

$$\alpha_1(L_a,\omega) = \frac{8\pi}{9(2L+1)} \sum_n \frac{\Delta E_{0n} |\langle n_0 L \| T_1 \| n L_a \rangle|^2}{\Delta E_{0n}^2 - \omega^2}, \qquad (7)$$

with $T_1 = \sum_{i=0}^3 q_i R_i Y_{10}(\hat{\mathbf{R}}_i)$ being the dipole transition operator, and

$$W(L,L_a) = (-1)^{L+L_a} \sqrt{\frac{30(2L+1)L(2L-1)}{(2L+3)(L+1)}}$$

$$\times \begin{Bmatrix} 1 & 1 & 2 \\ L & L & L_a \end{Bmatrix}. \qquad (8)$$

In the above, $|n_0 L\rangle$ is the initial state with principal quantum number n_0, angular momentum quantum number L, and energy E_0. The nth intermediate eigenfunction $|nL_a\rangle$, with principal quantum number n and angular momentum quantum number L_a, has energy E_n. The transition energy is $\Delta E_{0n} = E_n - E_0$. The q_i are the charges of the respective particles and the $\mathbf{R}_i$ are defined in Ref. [36]. In particular, for the case of $L = 0$,

$$\alpha_1(\omega) = \alpha_1(P,\omega), \qquad (9)$$
$$\alpha_1^T(\omega) = 0; \qquad (10)$$

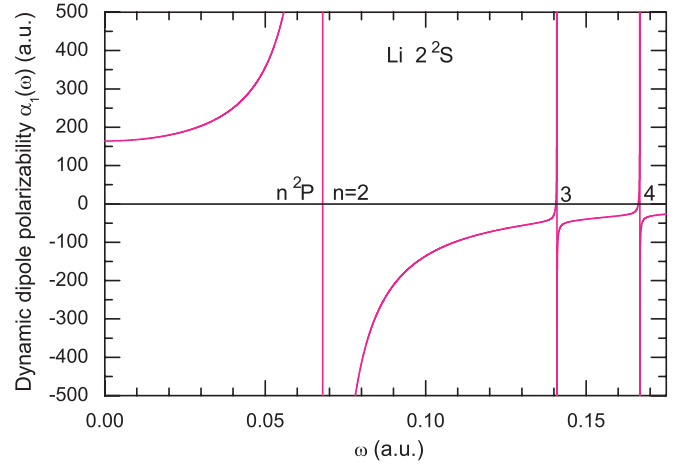FIG. 2. (Color online) Dynamic dipole polarizability $\alpha_1(\omega)$ of a ground-state Li atom. The singularities in the polarizability at the $2\,^2S \to n\,^2P$ frequencies are marked.

and for $L = 1$,

$$\alpha_1(\omega) = \alpha_1(S,\omega) + \alpha_1(P,\omega) + \alpha_1(D,\omega), \qquad (11)$$

$$\alpha_1^T(\omega) = -\alpha_1(S,\omega) + \tfrac{1}{2}\alpha_1(P,\omega) - \frac{1}{10}\alpha_1(D,\omega). \qquad (12)$$

In Eqs. (11) and (12), $\alpha_1(P,\omega)$ is the contribution from the even-parity configuration $(pp')P$. The scalar and tensor polarizabilities can be easily related to the polarizabilities of the magnetic sublevels, $\alpha_{1,M}(\omega)$:

$$\alpha_{1,0}(\omega) = \alpha_1(\omega) - 2\alpha_1^T(\omega),$$
$$\alpha_{1,\pm 1}(\omega) = \alpha_1(\omega) + \alpha_1^T(\omega). \qquad (13)$$

III. DYNAMIC POLARIZABILITY FOR $^\infty$Li ATOMS AND $^\infty$Be$^+$ IONS

A. Ground-state dynamic polarizabilities

Figure 2 shows the dynamic dipole polarizability of the Li ground state as a function of photon energy. The chief errors in the dynamic polarizability are related to the convergence of the $n\,^2P$ excited-state energies. The largest calculation used a basis with dimensions $(N_s, N_p) = (6412, 5761)$. The difference between the $\alpha_1(\omega)$ and polarizability computed with a basis $(N_s, N_p) = (4172, 3543)$ would be barely discernible in Fig. 2. The convergence of $\alpha_1(\omega)$ is best at photon energies far from the discrete excitation energies of the $n\,^2P$ excitations. The polarizability is very susceptible to small changes in the physical energies at photon energies close to the $n\,^2P$ excitation energies.

The uncertainties in the dynamic dipole polarizabilities of the Li ground state as well as the polarizabilities themselves are listed in Table II. All of the values listed are accurate to about ± 1 in the fifth digit for $\omega \leqslant 0.113\,88$ a.u. Some of the alternate calculations of the $\alpha_1(\omega)$ polarizabilities [20, 26,28,29,33] are listed in Table II. Dynamic polarizabilities from some less accurate calculations [30–32] have not been tabulated.

One feature of Table II is the excellent agreement with the MBPT-SD calculation of Safronova et al. [33]. The MBPT-SD

TABLE II. The dynamic dipole polarizabilities $\alpha_1(\omega)$ (in a.u.) for the Li ground state. The results of the fourth column include relativistic corrections. The numbers in parentheses for the second and third columns are the uncertainties in the last digits arising from incomplete convergence of the basis set. The uncertainties in the recommended (Rec.) values reflect additional uncertainties related to the relativistic correction.

	Hylleraas				TDGI	CI-Hylleraas	Model
ω	∞Li	^{7}Li	Rec. ^{7}Li	MBPT-SD [33]	[26,28]	[29]	Potential [20]
0.000 00	164.112(1)	164.161(1)	164.11(3)		163.6	164.1	164.14
0.005 00	164.996(1)	165.045(1)	165.00(3)		164.5	165.0	165.03
0.010 00	167.707(1)	167.758(1)	167.71(3)		167.2	167.7	167.74
0.020 00	179.517(1)	179.574(1)	179.52(3)		178.9	179.5	179.55
0.029 31	201.242(2)	201.313(1)	201.24(3)	201.0(7)			
0.030 00	203.438(1)	203.512(1)	203.44(3)		202.6	203.4	203.47
0.034 20	219.221(1)	219.307(1)	219.22(4)	219.0(8)			
0.040 00	250.265(1)	250.376(1)	250.26(4)		248.8	250.3	250.29
0.046 24	304.278(1)	304.441(1)	304.26(5)	304.0(8)			
0.050 00	356.077(1)	356.300(1)	356.05(6)		355.2	356.1	356.60
0.056 99	550.259(1)	550.790(1)	550.18(9)	549.7(1.1)			
0.060 00	741.165(2)	742.126(1)	741.00(12)		729.2		740.73
0.065 07	1984.577(1)	1991.488(1)	1983.11(31)	1983(3)			
0.070 00	−2581.603(2)	−2569.994(2)	−2584.54(40)		−2895.3		
0.075 92	−645.478(2)	−644.749(1)	−645.70(10)	−645.9(1.3)			
0.080 00	−415.067(1)	−414.763(1)	−415.17(7)		−427.1		
0.090 00	−211.518(2)	−211.439(1)	−211.55(3)		−216.5		
0.091 10	−199.941(1)	−199.868(1)	−199.97(3)	−200.1(0.8)			
0.100 00	−135.872(2)	−135.838(1)	−135.89(3)		−0.819		
0.113 88	−86.266(1)	−86.249(1)	−86.27(2)	−86.4(0.8)			
0.151 83	−38.210(9)	−38.204(9)	−38.22(1)	−38.4(1.1)			
0.160 00	−31.08(5)	−31.06(5)	−31.08(6)				

calculation and the present Hylleraas calculation are in perfect agreement when the MBPT-SD theoretical uncertainty is taken into consideration. While the MBPT-SD calculation is fully relativistic, its treatment of electron correlation is less exact than the present calculation. The MBPT-SD calculation also gives no consideration of finite-mass effects. Relativistic effects would tend to decrease $\alpha_1(\omega)$ at low ω, and the MBPT-SD calculation gives slightly smaller $\alpha_1(\omega)$ at low ω.

The older CI-Hylleraas calculation of values of Pipin and Bishop [29] compares excellently with the present, more modern, calculation. All digits in $\alpha_1(\omega)$ from the CI-Hylleraas calculation are in perfect agreement with the present Hylleraas calculation. The model potential polarizabilities of Cohen and Themelis [20] are also very close to the present dynamic polarizability. The Cohen-Themelis potential was constructed using a Rydberg-Klein-Rees (RKR) inversion method. The time-dependent gauge-invariant (TDGI) polarizabilities of Mérawa *et al.* [26,28] are only accurate to 0.5% or larger. The moderate accuracy of TDGI calculations has also been noted in calculations of the static polarizabilities [17].

The static polarizabilities for Be$^+$ in the infinite-mass approximation have been presented recently [23]. The present calculation represents an extension of this earlier calculation since finite-mass effects are now included. The dynamic dipole polarizabilities listed in Table III includes transition frequencies that extend well into the ultraviolet region. The most accurate of the few alternate calculations should be the

CI-Hylleraas calculation of Muszynska *et al.* [32]. However, it gives an $\alpha_1(\omega)$ that is about 1% smaller than the present polarizability. Space limitations precluded tabulation of the TDGI polarizability [28]. The TDGI polarizability was of only moderate accuracy with errors of about 2% for $\omega \leqslant 0.6$ a.u. The uncertainty in the present polarizability is about 10^{-4} a.u. for photon energies lower than 0.40 a.u., but has increased to 10^{-2} a.u. at $\omega = 0.50$ a.u.

The dynamic polarizabilities for the Li and Be$^+$ ground states are depicted in Figs. 2 and 3. There are obvious similarities in shapes of the two $\alpha_1(\omega)$ curves but with the Li polarizability being about 5–10 times larger in magnitude at comparable values of $\omega/\omega_{2s\to2p}$. One difference between the two curves is that Be$^+$ has zeros in $\alpha_1(\omega)$ at a discernible frequency difference before the $3\,^2P$ and $4\,^2P$ excitations while the $\alpha_1(\omega)$ negative-to-positive crossovers for Li occur much closer to the transition frequencies.

B. Excited-state dynamic polarizabilities

The scalar and tensor dipole polarizabilities for the excited $2\,^2P$ state of the Li atom are listed in Table IV. As far as we know, the present calculations are the only dynamic polarizabilities presented for this state. The structure of the dynamic polarizability is complicated since both downward and upward transitions leads to singularities. This is seen most clearly in Fig. 4, which plots the polarizabilities for photon energies up to 0.10 a.u. The tensor polarizability is generally small except in the vicinity of the $2\,^2S$, $3\,^2S$, and

TABLE III. Dynamic dipole polarizabilities $\alpha_1(\omega)$ (in a.u.) for the Be$^+$ ground state. The results of the fourth column incorporate relativistic effects. The numbers in parentheses are the uncertainties in the last digits arising from incomplete convergence of the basis set. The recommended (Rec.) polarizabilities in the fourth column reflect uncertainties other than purely computational.

	Hylleraas			CI-Hylleraas
ω (a.u.)	∞Be$^+$	^{9}Be$^+$	Rec. ^{9}Be$^+$	[32]
0.00	24.496 6(1)	24.506 4(1)	24.489(4)	24.3
0.01	24.608 8(1)	24.618 7(1)	24.601(4)	24.4
0.02	24.951 8(1)	24.962 0(1)	24.943(4)	24.7
0.04	26.429 1(1)	26.440 4(1)	26.419(4)	26.2
0.06	29.339 0(1)	29.352 8(1)	29.325(5)	29.1
0.08	34.735 8(1)	34.755 0(1)	34.715(6)	34.3
0.10	45.650 9(1)	45.683 6(1)	45.609(7)	44.9
0.12	74.785 7(1)	74.872 4(1)	74.656(12)	
0.15	$-367.870\ 8(2)$	$-365.803\ 0(3)$	$-371.860(60)$	
0.18	$-43.203\ 8(1)$	$-43.174\ 5(1)$	$-43.273(7)$	
0.20	$-25.319\ 5(1)$	$-25.309\ 0(1)$	$-25.348(4)$	
0.30	$-5.796\ 7(1)$	$-5.795\ 1(1)$	$-5.801(2)$	
0.40	$-0.291\ 2(1)$	$-0.287\ 3(1)$	$-0.2961(2)$	
0.50	$-2.149(7)$	$-2.161(7)$	$-2.164(8)$	

$3\,^2D$ transitions. The tensor polarizability can become large when a single transition tends to dominate Eq. (12). The scalar and tensor polarizabilities tend to be opposite in sign. The main contribution to the polarizabilities comes from transitions to
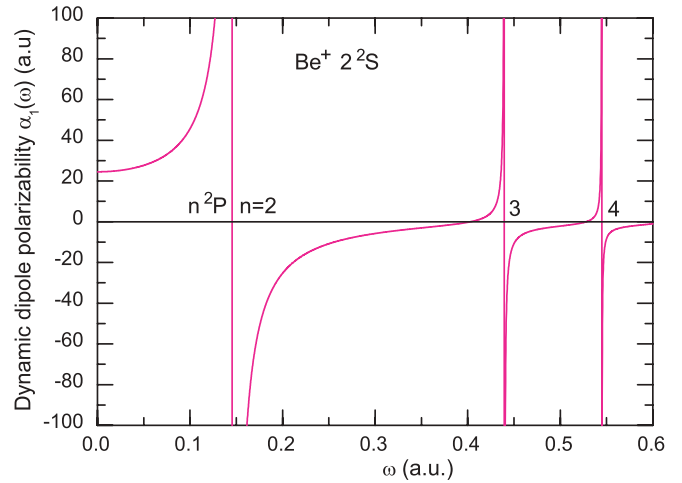

FIG. 3. (Color online) The dynamic dipole polarizability $\alpha_1(\omega)$ for the ground state of Be$^+$. The singularities in the polarizability at the $2\,^2S \rightarrow n\,^2P$ frequencies are marked.

the S and D states. The coefficients in the sum rules, Eqs. (11) and (12), for these terms are opposite in sign.

The dynamic polarizabilities for the Be$^+$ $2\,^2P$ state are also tabulated in Table IV and depicted in Fig. 5 for photon frequencies below 0.40 a.u. There are three resonances in this frequency range. The scalar and tensor dynamic polarizabilities are similar in shape but with the opposite sign. As far as we know, there has been no previous calculation of the $2\,^2P$ state dynamic polarizability.

TABLE IV. The dynamic dipole polarizabilities of the $2\,^2P$ state of Li and Be$^+$. Both the scalar and tensor polarizabilities are tabulated. The numbers in parentheses are the uncertainties in the last digits arising from incomplete convergence of the basis set. Values without uncertainties have no numerical uncertainties in any of the quoted digits. The recommended (Rec.) polarizabilities in the sixth and seventh columns have estimated corrections from relativistic effects. The recommended polarizabilities reflect uncertainties other than purely computational.

|	∞Li		^{7}Li		Rec. ^{7}Li	
ω (a.u.)	α_1	α_1^T	α_1	α_1^T	α_1	α_1^T
0.00	126.945 8(3)	1.621 4(3)	126.947 2(5)	1.635 1(2)	126.970(4)	1.612(4)
0.01	129.249 1(5)	1.403 5(2)	129.250 1(5)	1.417 8(2)	129.273(4)	1.393(4)
0.02	136.837 1(5)	0.530 2(3)	136.837 2(5)	0.546 3(5)	136.864(4)	0.518(4)
0.03	152.469(1)	$-2.091(1)$	152.468(2)	$-2.070(1)$	152.503(4)	$-2.106(4)$
0.04	185.542(5)	$-11.722(5)$	185.535(5)	$-11.691(5)$	185.593(6)	$-11.747(6)$
0.05	301.24(8)	$-82.33(9)$	301.23(9)	$-82.27(8)$	301.33(10)	$-82.38(10)$
0.06	$-119.1(5)$	446.7(5)	$-119.3(5)$	446.9(5)	$-119.0(6)$	446.6(6)
0.07	1804.5(1)	$-904.2(2)$	1801.2(1)	$-900.34(5)$	1806.2(2)	$-905.2(2)$
0.08	$-593.1(2)$	$-43.5(4)$	$-592.7(3)$	$-43.6(5)$	$-592.6(5)$	$-43.4(5)$
	∞Be$^+$		^{9}Be$^+$		Rec. ^{9}Be$^+$	
0.00	2.024 76(1)	5.856 012(1)	2.023 19(1)	5.858 938(1)	2.028 5(10)	5.852 8(10)
0.01	1.997 55(1)	5.890 887(1)	1.995 95(1)	5.893 842(1)	2.001 3(10)	5.887 6(10)
0.02	1.913 89(1)	5.997 630(1)	1.912 21(1)	6.000 672(1)	1.917 8(12)	5.994 2(12)
0.05	1.231 44(1)	6.845 876(1)	1.229 05(1)	6.849 643(1)	1.236 3(13)	6.841 5(13)
0.10	$-3.881\ 78(1)$	12.617 90	$-3.890\ 80(1)$	12.628 42	$-3.866\ 6(15)$	12.603 3(13)
0.14	$-94.714\ 54$	104.485 95	$-95.247\ 6$	105.020 73	$-93.787\ 3(16)$	103.559 2(16)
0.20	26.150 5(1)	$-12.948\ 1(2)$	26.149 9(1)	$-12.945\ 1(1)$	26.161(17)	$-12.958(12)$
0.25	48.59(5)	$-26.10(1)$	48.61(5)	$-26.11(1)$	48.62(6)	$-26.17(1)$
0.28	52.09(1)	$-3.43(1)$	52.10(1)	$-3.44(1)$	52.07(1)	$-3.45(1)$
0.32	$-49.87(1)$	4.413(1)	$-49.85(1)$	4.412(1)	$-49.89(1)$	4.40(1)
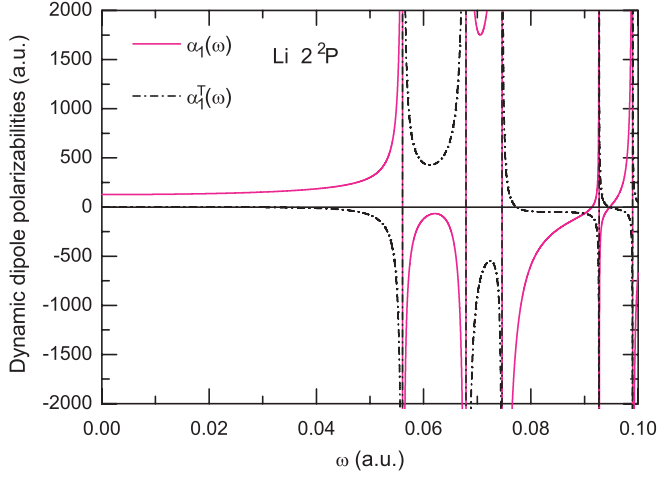
FIG. 4. (Color online) The dynamic polarizabilities $\alpha_1(\omega)$ and $\alpha_1^T(\omega)$ (in a.u.) of the Li $2\,^2P$ state for photon frequencies below 0.10 a.u. The scalar polarizability is given by the solid line while the tensor polarizability is given by the chain curve.

C. Static $2\,^2S \to 2\,^2P$ Stark shift

The static Stark shift δG for the change in the $2\,^2S \to 2\,^2P$ energy interval in an electric field of strength F is written as

$$\delta G_{2s\text{-}2p,M} = -\tfrac{1}{2} F^2 (\alpha_{2s} - \alpha_{2p,M})$$
$$- \tfrac{1}{24} F^4 (\gamma_{2s} - \gamma_{2p,M}) + \dots, \qquad (14)$$

where γ is the hyperpolarizability. The Stark shift depends on the magnetic quantum number M of the $2\,^2P$ state. The relative size of $\Delta\alpha$ and $\Delta\gamma$ determines the extent to which the Stark shift is influenced by the hyperpolarizability at high field strengths. The relative importance of $\Delta\alpha$ and $\Delta\gamma$ is given by the ratio

$$X = \frac{F^2(\gamma_{2s} - \gamma_{2p,M})}{12(\alpha_{2s} - \alpha_{2p,M})} = \frac{F^2 \Delta\gamma}{12\Delta\alpha}. \qquad (15)$$
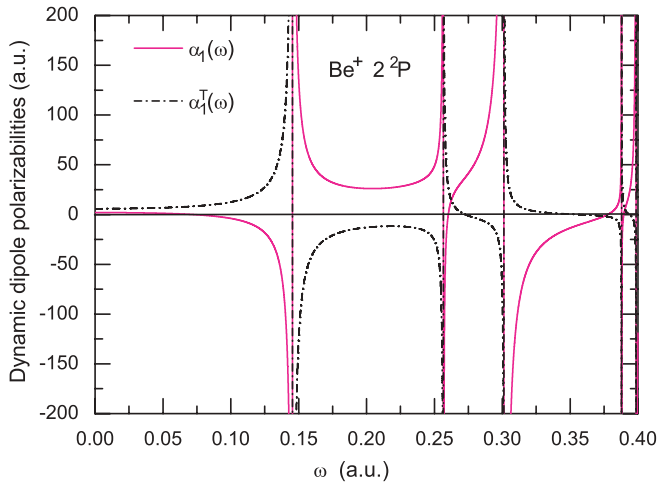

FIG. 5. (Color online) The dynamic polarizabilities $\alpha_1(\omega)$ and $\alpha_1^T(\omega)$ (in a.u.) of the Be$^+$ $2\,^2P$ state for photon frequencies below 0.40 a.u. The scalar polarizability is given by the solid line while the tensor polarizability is given by the chain curve.
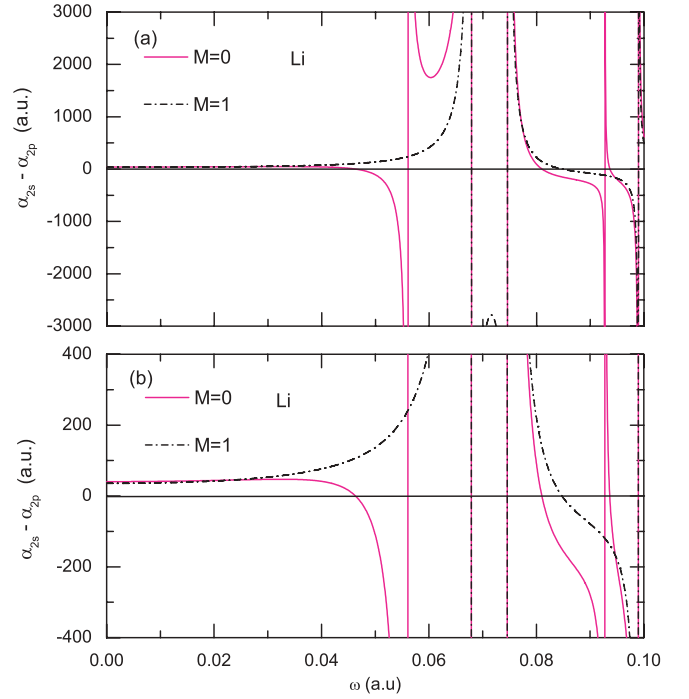

FIG. 6. (Color online) The polarizability difference between the $2\,^2S$ and $2\,^2P$ states of Li. Polarizability differences are shown for $M = 0$ and $M = 1$.

Using the static polarizability and static hyperpolarizability for the Li atom results in $\Delta\alpha = 37.1$ and $\Delta\gamma = 9.99 \times 10^6$ giving $X = 0.0001$ at $F = 6.67 \times 10^{-5}$ a.u. (344 kV/cm) and $X = 0.001$ at $F = 2.11 \times 10^{-4}$ a.u. (1087 kV/cm). These estimates of the critical field strength where the quadratic Stark shift is valid depend slightly on the magnetic quantum number, and exact values can be determined by using M-dependent polarizabilities. Stark shifts of higher order than the hyperpolarizability can be comfortably ignored at the 0.01% level, provided the field strength is less than 1100 kV/cm. The static Stark shift for Be$^+$ is not interesting since it is difficult to measure as a Be$^+$ ion immersed in a finite electric field is accelerated away from the finite-field region.

D. Dynamic $2\,^2S \to 2\,^2P$ Stark shift

The Li Stark shifts, $\alpha(2s) - \alpha(2p_M)$, are plotted as a function of frequency in Fig. 6. It is seen that there are magic wavelengths for $M = 0$ just below the $2\,^2P \to 3\,^2S$ threshold and between the $2\,^2S \to 2\,^2P$ and $2\,^2P \to 3\,^2D$ thresholds. The actual energies for which the polarizability difference is zero are given in Table V. The Stark shifts get very large for frequencies between 0.058 and 0.070 a.u.

The Be$^+$ Stark shifts, $\alpha(2s) - \alpha(2p_M)$, are plotted as a function of frequency in Fig. 7. The Stark shifts are much smaller in magnitude than the Li atom shifts. One difference from Li is that the Be$^+$ shift has no zero for energies below the $2\,^2S \to 2\,^2P$ threshold. The first zero in the Stark shift (excepting those related to a singularity) is at 0.263 a.u.

TABLE V. The photon energies for which there is no Stark shift for the $2\,^2S \rightarrow 2\,^2P$ transition. Underlined digits indicate uncertain digits arising from lack of basis set convergence. Digits in brackets indicate possible uncertainties associated with relativistic corrections in the recommended (Rec.) values.

System	$M = 0$	$M = 1$
$^\infty$Li	0.046 317 680 $\underline{6}$	0.084 763 957 $\underline{1}$
	0.081 021 795 $\underline{5}$	
	0.093 664 330 $\underline{5}$	
^{7}Li	0.046 335 687 $\underline{8}$	0.084 766 087 $\underline{0}$
	0.081 024 478 $\underline{9}$	
	0.093 661 899 $\underline{1}$	
Rec. ^{7}Li	0.046 297(4)	0.084 756(2)
	0.081 014(2)	
	0.093 661 3(2)	
$^\infty$Be$^+$	0.262 920 267 $\underline{8}$	0.378 457 000 $\underline{4}$
	0.370 371 502 $\underline{7}$	
	0.390 752 146 $\underline{3}$	
^{9}Be$^+$	0.262 917 360 $\underline{3}$	0.378 451 843 $\underline{7}$
	0.370 279 952 $\underline{2}$	
	0.390 455 356 $\underline{8}$	
Rec. ^{9}Be$^+$	0.262 895 6(7)	0.378 443(2)
	0.370 274(1)	
	0.390 454 6(2)	

E. Analytic representation

The utility of the present calculations can be increased by constructing a closed-form expression for the dynamic polarizability. This is done by retaining the first 3 terms in Eq. (7) explicitly and then expanding the energy denominator in the remainder. The expressions explicitly include oscillator strengths up to the $n = 4$ principal quantum numbers. The closed form expression is

$$\alpha_1(\omega) = \left(\sum_{n=2}^{4} \frac{f_{2s \rightarrow np}}{\Delta E_{2snp}^2 - \omega^2} \right) + S(-2) + \omega^2 S(-4)$$
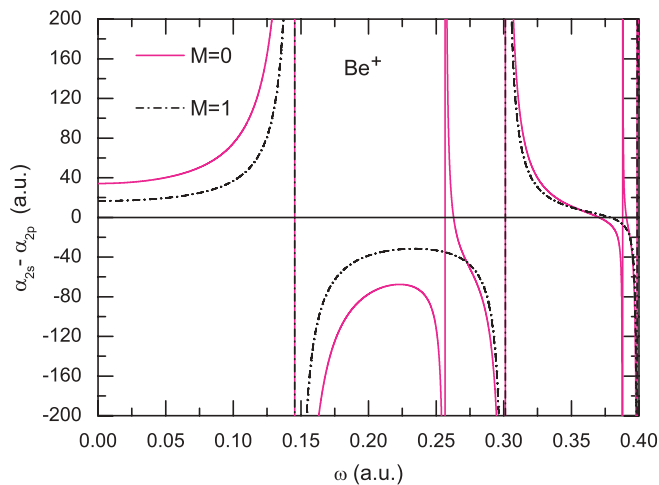$$+ \omega^4 S(-6) + \cdots + \omega^{14} S(-16) + C(\omega), \quad (16)$$

FIG. 7. (Color online) The polarizability difference between the $2\,^2S$ and $2\,^2P$ states of Be$^+$. Polarizability differences are shown for $M = 0$ and $M = 1$.

where

$$S(-m) = \sum_{n=5} \frac{f_{2s \rightarrow np}}{(\Delta E_{2snp})^m}, \quad (17)$$

$$C(\omega) = \frac{\eta_1 \omega^{16} S(-16)}{1 - \eta_1 \omega^2}. \quad (18)$$

Here, $f_{2s \rightarrow np}$ are the dipole oscillator strengths for the $2\,^2S \rightarrow n\,^2P$ transitions with transition energies $\Delta E_{2snp} = E_{np} - E_{2s}$. The oscillator strength is defined as

$$f_{n_0 L \rightarrow nL'} = \frac{8\pi}{(2\ell + 1)^2 (2L + 1)} \Delta E_{n_0 LnL'} |\langle n_0 L \| T_\ell \| nL' \rangle|^2. \quad (19)$$

The $S(-n)$ are the Cauchy moments of the remainder of the oscillator-strength distribution and are independent of ω. The term $C(\omega)$ is an approximate term to represent the summation from the term $S(-18)$ to $S(\infty)$. The ratio $\eta_1 = S(-n-2)/S(-n)$ is assumed to be constant and its value is set to $S(-16)/S(-14)$. Numerical values of the various constants in Eq. (16) can be found in Table VI. Inclusion of the remainder term has greatly increased the precision of the analytic fit to the exact dynamic polarizability.

The analytic representation for the Li $2\,^2S$ state is accurate to 0.01 a.u. for $\omega \leqslant 0.1612$ a.u. and to an accuracy of 0.1 a.u. for $\omega \leqslant 0.1728$ a.u. The dynamic polarizability for the Be$^+$ $2\,^2S$ state maintains its accuracy over a larger ω range. It is accurate to 0.001 a.u. for $\omega \leqslant 0.543$ a.u., to 0.01 a.u. for $\omega \leqslant 0.586\,05$ a.u., and to 0.1 a.u. for $\omega \leqslant 0.6$ a.u.

The presence of zeros in the dynamic polarizability near the singularities means that the relative error in the analytic representation can get very large in a frequency range very close to the zeros. Neglecting these localized regions with anomalously high relative uncertainties, the relative difference between the analytic representation and actual dynamic polarizability for the Li $2\,^2S$ state was less than 0.001% for $\omega \leqslant 0.1399$ a.u., 0.01% for $\omega \leqslant 0.1551$ a.u., and 0.1% for $\omega \leqslant 0.1651$ a.u. The relative difference for the Be$^+$ $2\,^2S$ state obtained by the variational Hylleraas method was less than 0.001% for $\omega \leqslant 0.4737$ a.u., 0.01% for $\omega \leqslant 0.5067$ a.u., and 0.1% for $\omega \leqslant 0.525\,75$ a.u. The inclusion of the remainder term $C(\omega)$ improved the accuracy of the analytic representation by one or two orders of magnitude within the frequency range listed above.

The dynamic dipole polarizabilities of the $2\,^2P$ states of Li and Be$^+$ have both scalar $\alpha_1(\omega)$ and tensor $\alpha_1^T(\omega)$ parts. The scalar part can be written as

$$\alpha_1(\omega) = \sum_{n=2}^{4} \frac{f_{2p \rightarrow ns}}{\Delta E_{2pns}^2 - \omega^2} + \sum_{n=3}^{4} \frac{f_{2p \rightarrow nd}}{\Delta E_{2pnd}^2 - \omega^2}$$
$$+ S(-2) + \omega^2 S(-4) + \omega^4 S(-6) + \cdots$$
$$+ \omega^{14} S(-16) + C(\omega), \quad (20)$$

where

$$S(-m) = \sum_{n=5} \frac{f_{2p \rightarrow ns}}{(\Delta E_{2pns})^m} + \sum_{n'} \frac{f_{2p \rightarrow n'P}}{(\Delta E_{2pn'P})^m}$$
$$+ \sum_{n=5} \frac{f_{2p \rightarrow nd}}{(\Delta E_{2pnd})^m}. \quad (21)$$

TABLE VI. The parameters for the calculation of the $2\,^2S$-state frequency-dependent polarizabilities of Li and Be⁺. The numbers in the square brackets denote powers of 10. The recommended (Rec.) results of the fourth and the seventh columns incorporate relativistic corrections.

Parameter	∞Li	^{7}Li	Rec. ^{7}Li	∞Be⁺	^{9}Be⁺	Rec. ^{9}Be⁺
$f_{2s\to2p}$	0.746 956 855 381	0.746 961 871 867	0.747 011 776 131	0.498 067 422 721	0.498 083 382 699	0.498 227 010 322
ΔE_{2s2p}	0.067 903 791 567	0.067 894 172 078	0.067 906 05	0.145 429 884 364	0.145 403 572 344	0.145 478 06
$f_{2s\to3p}$	0.004 731 019 443	0.004 737 600 312	0.004 728 028 090	0.083 243 986 131	0.083 288 941 464 7	0.083 209 271 939
ΔE_{2s3p}	0.140 909 212 964	0.140 896 165 068	0.140 906 40	0.439 629 051 730	0.439 596 005 937	0.439 665 21
$f_{2s\to4p}$	0.004 960 028 680	0.004 964 714 658		0.040 874 056 901	0.040 896 543 934	
ΔE_{2s4p}	0.166 756 175 058	0.166 742 266 938		0.546 967 693 380	0.546 934 227 760	
$S(-2)$	1.697 71	1.698 63		0.379 627	0.379 781	
$S(-4)$	21.871 4	21.888 8		0.513 938	0.514 207	
$S(-6)$	428.809	429.237		0.979 476	0.980 088	
$S(-8)$	9.693 64[3]	9.705 02[3]		2.053 22	2.054 69	
$S(-10)$	2.370 08[5]	2.373 25[5]		4.521 45	4.525 08	
$S(-12)$	6.080 98[6]	6.090 06[6]		10.247 3	10.256 4	
$S(-14)$	1.610 32[8]	1.612 96[8]		23.636 8	23.659 6	
$S(-16)$	4.357 60[9]	4.365 37[9]		55.128 0	55.185 2	
η_1	27.060 5	27.064 3		2.332 29	2.332 46	

The $2p \to n'P$ excitation involves a core excitation and the intermediate state is an unnatural parity $^2P^e$ state. The tensor part is

$$\alpha_1^T(\omega) = -\sum_{n=2}^{4} \frac{f_{2p\to ns}}{\Delta E_{2pns}^2 - \omega^2} - \frac{1}{10}\sum_{n=3}^{4} \frac{f_{2p\to nd}}{\Delta E_{2pnd}^2 - \omega^2}$$
$$+ S^T(-2) + \omega^2 S^T(-4) + \omega^4 S^T(-6) + \cdots$$
$$+ \omega^{14} S^T(-16) + C^T(\omega), \qquad (22)$$

where

$$S^T(-m) = -\sum_{n=5} \frac{f_{2p\to ns}}{(\Delta E_{2pns})^m} + \frac{1}{2}\sum_{n'} \frac{f_{2p\to n'P}}{(\Delta E_{2pn'P})^m}$$
$$- \frac{1}{10}\sum_{n=5} \frac{f_{2p\to nd}}{(\Delta E_{2pnd})^m}, \qquad (23)$$

$$C^T(\omega) = \frac{\eta_1^T \omega^{16} S^T(-16)}{1 - \eta_1^T \omega^2}, \qquad (24)$$

where $f_{2p\to mL_1}$ means the oscillator strength from the $2p$-state to the mL_1-state transition. The coefficients $S^T(-2)$, $S^T(-4)$, $S^T(-6), \ldots$ correspond to the $\omega^0, \omega^2, \omega^4, \ldots$ terms of the tensor part. The remainder term $C^T(\omega)$ is an approximate expression to take into account the $S^T(-18) \to S^T(\infty)$ summations. The factor η_1^T is set to be $\eta_1^T = S(-16)/S(-14)$. All parameters in the analytic representation are given in Table VII.

The first two terms of Eqs. (20) and (22) include five resonances which make the major contribution to the polarizability, with the second term involving excitations to D states being the most important. This is clearly seen in the Li $\alpha_1(\omega)$ of 185.542(5) a.u. at $\omega = 0.04$ a.u. The contribution of the first summation of Eq. (20) was -8.8717 a.u., while the second summation contributed 175.8241 a.u. The value given by Eq. (20) was 185.5378 a.u., which agrees with the exact value at the level of 0.0004%.

The analytic representation for the scalar polarizability $\alpha_1(\omega)$ of the Li $2\,^2P$ state is accurate to 0.01 a.u. for $\omega \leqslant$ 0.0855 a.u. and to 0.1 a.u. for $\omega \leqslant 0.0937$ a.u. The analytic representation for the tensor polarizability $\alpha_1^T(\omega)$ is accurate to 0.01 a.u. for $\omega \leqslant 0.0926$ a.u. and to 0.10 a.u. for $\omega \leqslant 0.1$ a.u.

The relative error in the analytic representation of $\alpha_1(\omega)$ for the $2\,^2P$ state of the Li atom is less than 0.001% for $\omega \leqslant 0.082$ a.u., 0.01% for $\omega \leqslant 0.0871$ a.u., and 0.1% for $\omega \leqslant 0.0906$ a.u. The relative error of the analytic representation for $\alpha_1^T(\omega)$ is less than 0.001% for $\omega \leqslant 0.0815$ a.u., 0.01% for $\omega \leqslant 0.0932$ a.u., and 0.1% for $\omega \leqslant 0.0995$ a.u.

The dynamic polarizability of the Be⁺ $2\,^2P$ state maintains its accuracy over a larger range of ω. It is accurate to 0.001 a.u. for $\omega \leqslant 0.3513$ a.u., to 0.01 a.u. for $\omega \leqslant 0.3837$ a.u., and 0.1 a.u. for $\omega \leqslant 0.4111$ a.u. The absolute error for $\alpha_1^T(\omega)$ is 0.001 a.u. for $\omega \leqslant 0.3788$ a.u., 0.01 a.u. for $\omega \leqslant 0.4077$ a.u., and 0.1 a.u. for $\omega \leqslant 0.4291$ a.u.

The relative error between the analytic representation and Hylleraas values of $\alpha_1(\omega)$ for the Be⁺ $2\,^2P$ state is less than 0.001% for $\omega \leqslant 0.332$ a.u., 0.01% for $\omega \leqslant 0.3536$ a.u., and 0.1% for $\omega \leqslant 0.3708$ a.u. The relative error for $\alpha_1^T(\omega)$ of the Be⁺ $2\,^2P$ state is less than 0.001% for $\omega \leqslant 0.3265$ a.u., 0.01% for $\omega \leqslant 0.3434$ a.u., and 0.1% for $\omega \leqslant 0.3534$ a.u.

IV. FINITE-MASS CORRECTIONS

The effect of the finite mass was to decrease the Li atom and Be⁺ ion binding energies listed in the Table I. Therefore, it is not surprisingly that the $\omega = 0$ polarizabilities of the Li and Be⁺ ground states are increased in Tables II and III. The overall changes of the $\omega = 0$ polarizabilities are 0.03% and 0.04% for Li and Be⁺ respectively. The finite-mass polarizabilities are larger than the infinite-mass values at $\omega = 0$ a.u. These differences can be taken as indicative of the overall change in the polarizabilities at finite frequencies below the first excitation threshold. The differences are naturally larger near thresholds.

The finite-mass effect for the Li $2\,^2P$ state increased its polarizability by 0.001% (Table IV) while decreasing the

TABLE VII. The parameters defining the frequency-dependent polarizabilities of the $2\,^2P$ state of Li and Be$^+$. The numbers in the square brackets denote powers of 10. The recommended (Rec.) results of the fourth and the seventh columns incorporate relativistic effects.

Parameter	∞Li	^{7}Li	Rec. ^{7}Li	∞Be$^+$	^{9}Be$^+$	Rec. ^{9}Be$^+$
$f_{2p\rightarrow2s}$	−0.248 985 618 454	−0.248 987 290 622	−0.249 003 925 38	−0.166 022 474 240	−0.166 027 794 233	−0.166 075 670 107
ΔE_{2p2s}	−0.067 903 791 567	−0.067 894 172 078	−0.067 906 050	−0.145 429 884 364	−0.145 403 572 344	−0.145 478 060 000
$f_{2p\rightarrow3s}$	0.110 578 835 460	0.110 575 403 831	0.110 589 306 872	0.064 385 095 804	0.064 385 347 515	0.064 407 168 594
ΔE_{2p3s}	0.056 059 306 121	0.056 058 468 507	0.056 054 150	0.256 561 561 765	0.256 561 980 308	0.256 536 125 000
$f_{2p\rightarrow4s}$	0.014 979 087 136	0.014 981 586 569		0.012 876 689 561	0.012 879 003 186	
ΔE_{2p4s}	0.092 714 410 055	0.092 711 788 029		0.387 472 175 091	0.387 469 829 948	
$f_{2p\rightarrow3d}$	0.638 568 044 661	0.638 583 007 678	0.638 583 083 728	0.631 981 700 709	0.632 059 480 294	0.632 047 210 702
ΔE_{2p3d}	0.074 632 989 884	0.074 630 453 329	0.074 630 150	0.301 279 233 806	0.301 276 362 793	0.301 291 440 000
$f_{2p\rightarrow4d}$	0.122 746 501 135	0.122 756 411 337		0.122 711 398 708	0.122 734 598 764	
ΔE_{2p4d}	0.098 967 235 189	0.098 962 799 378		0.398 640 164 736	0.398 631 384 564	
$S(-2)$	16.840 8	16.844 7		1.075 95	1.076 28	
$S(-4)$	974.832	975.135		3.695 33	3.696 58	
$S(-6)$	6.408 29[4]	6.410 83[4]		14.942 2	14.947 9	
$S(-8)$	4.484 04[6]	4.486 20[6]		64.383 8	64.411 3	
$S(-10)$	3.261 08[8]	3.262 95[8]		288.547	288.684	
$S(-12)$	2.434 29[10]	2.435 92[10]		1328.18	1328.87	
$S(-14)$	1.851 41[12]	1.852 82[12]		6232.21	6235.79	
$S(-16)$	1.427 96[14]	1.429 18[14]		296 67.5	296 85.9	
η_1	77.128 2	77.135 4		4.760 34	4.760 58	
$S^T(-2)$	−2.730 75	−2.731 18		−0.156 423	−0.156 454	
$S^T(-4)$	−154.670	−154.702		−0.544 987	−0.545 110	
$S^T(-6)$	−9.881 99[3]	−9.884 58[3]		−2.109 90	−2.110 44	
$S^T(-8)$	−6.716 03[5]	−6.718 18[5]		−8.715 72	−8.718 24	
$S^T(-10)$	−4.735 61[7]	−4.737 42[7]		−37.508 3	−37.520 6	
$S^T(-12)$	−3.422 63[9]	−3.424 17[9]		−166.164	−166.226	
$S^T(-14)$	−2.519 02[11]	−2.520 34[11]		−752.681	−753.003	
$S^T(-16)$	−1.880 83[13]	−1.881 97[13]		−3471.37	−3473.06	
η_1^T	74.665 1	74.671 3		4.612 01	4.612 28	

polarizability for the Be$^+$ $2\,^2P$ state (Table IV) by 0.08%. This behavior for Be$^+$ is due to the $2\,^2P \rightarrow 2\,^2S$ downward transition. The increased negative contribution from this transition is enough to outweigh the increased positive contributions from transitions to more highly excited states.

As a general rule, the magnitude of the polarizabilities for both upward and downward transitions increase for the finite-mass calculations. The residual Cauchy moments $S(-n)$ in Table VI and Table VII all increase for the finite-mass calculations since these are computed exclusively from upward transitions.

V. OTHER EFFECTS AND UNCERTAINTIES

A. Estimate of relativistic effects

The major omission from the present calculation is the inclusion of relativistic effects. The larger part of the energy difference between the present finite-mass calculations and the experimental binding energies in Table I is due to the omission of relativistic effects. Relativistic effects will alter the polarizability calculation in two ways. First, the energy differences will be changed. Generally, the binding energies of all states can be expected to be slightly larger. Secondly, there will be some changes in the reduced matrix elements. The wave functions for the $n\,^2S$ and $n\,^2P$ states can be expected to be slightly more compact since they are more tightly bound.

Correcting for the relativistic energy is simply a matter of replacing the theoretical energies in the sum rules by the experimental values. The spin-orbit weighted averages were used for states with $L \geqslant 1$. The corrections to the transition matrix elements are made by recourse to calculations using a semiempirical model potential that supplements the potential field of a frozen Hartree-Fock (HF) core with a tunable polarization potential [21,23,37]. Polarizabilities for Li and Be$^+$ computed with this approach reproduce the Hylleraas calculation at the 0.1%-accuracy level [17,21,23].

The method used to estimate the relativistic effect upon matrix elements relies on comparing two very similar

TABLE VIII. Experimental C_3 values from analysis of the Li$_2$ spectrum and C_3 values from the Hylleraas calculations.

Source	Value
Li$_2$ spectrum [39], C_6 fixed from [19]	11.002 2(24)
Li$_2$ spectrum [8], C_6 fixed from [19]	11.002 41(23)
Li$_2$ spectrum [8], C_6 fixed from [21]	11.002 40(23)
Hylleraas ∞Li	11.000 221
Hylleraas ^{7}Li	11.001 853
Hylleraas ^{7}Li: Recommended	11.000 7

calculations. One calculation has its polarization potentials tuned to reproduce the finite-mass energies of Table I. The other calculation is tuned to give the experimental energies. The matrix elements for the low-lying transitions that dominate the dynamic polarizabilities are then compared. The differences between the "finite-mass" calculation and the "experimental" calculations are then determined. These changes in the matrix elements are then applied as corrections to the set of Hylleraas matrix elements. The only matrix elements that are changed are those involving transitions inside the $2\,^2L$ and $3\,^2L$ level space. Transitions to these states dominate the $2\,^2S$ and $2\,^2P$ polarizabilities. The actual change in the Li $2\,^2S \rightarrow 2\,^2P$ matrix element was a reduction of 0.0054%. The reduction in the Be$^+$ $2\,^2S \rightarrow 2\,^2P$ matrix element was 0.011%.

Using the new set of corrected matrix elements gives a ground state polarizability of 164.114 a.u. (Table I). This represents a reduction of the polarizability by 0.047 a.u. A coupled-cluster calculation of the Li ground state estimated that relativistic effects reduced its polarizability by 0.06 a.u. [38]. The static polarizability of the $2\,^2P$ state of ^{7}Li; namely 126.947 a.u., was increased to 126.970 a.u. (Table IV). This gives a Stark shift of -37.144 a.u., which is in agreement with the experiment of Hunter *et al.* [13] which gave $-37.14(2)$ for the ^{7}Li $2\,^2S$–$2\,^2P_{1/2}$ Stark shift. Another calculation was made to check the $2\,^2P_{1/2}$:$2\,^2P_{3/2}$ polarizability difference. The MBPT-SD calculation gave a difference of 0.015 a.u. [22]. Doing two calculations tuned to give a $2\,^2P$ spin-orbit splitting of 1.77×10^{-6} a.u. (the energy splitting in the MBPT-SD calculation [22]) gave a polarizability difference of 0.0145 a.u.. The energy splitting in the MBPT-SD calculation [22] gave a polarizability difference of 0.0145 a.u. A further test was made by examination of the line strengths of the Si^{3+} $3\,^2S$–$3\,^2P$ spin-orbit doublet. An MBPT-SD calculation gave a line-strength ratio of 1.000 524 (once angular momentum factors were removed) [40]. Turning the core potential in a semiempirical model based on the Schrödinger equation [40] gave a value of 1.000 618. The available evidence supports the conjecture that it is possible to use the energy differences between the Hylleraas and experimental energies to get an initial estimate of relativistic corrections for other properties such as the polarizability. The uncertainty in the correction would seem to be about 20%. To a certain extent, the cancellations involved in adding the finite-mass and relativistic corrections together leads to polarizabilities that are close to the infinite-mass polarizabilities.

The static polarizability of the Be$^+$ ground state was reduced from 24.506 to 24.489 a.u. This represents a reduction of 0.4%. However, the static scalar polarizability of the $2\,^2P$ state increased from 2.0231 to 2.0285 a.u., an increase of 0.24%. The static tensor polarizability changed from 5.8589 to 5.8528 a.u. The heavier mass and larger nuclear charge means relativistic effects are substantially larger than finite-mass corrections.

Dynamic polarizabilities and their analytic representations from the set of matrix elements with the estimate of the relativistic effects are listed in Tables II–VII as the recommended values. The changes to analytic representation only involved changes in the oscillator strength and energy differences for a few states.

B. $2\,^2S \rightarrow 2\,^2P$ matrix element and uncertainties

Recently Le Roy *et al.* [8] analyzed the ro-vibrational spectrum of the lithium dimer obtaining an estimate for the C_3 parameter describing the long range C_3/R^3 potential of the A state that dissociates to the $2\,^2S$ and $2\,^2P$ states. The C_3 parameter can be related to the $2\,^2S$–$2\,^2P$ multiplet strength. The determination of Le Roy *et al.* represented an order-of-magnitude improvement in precision over any previous determination of C_3.

The current value of $C_3 = 11.0007$ a.u., computed with relativistic corrections, is about 0.0155% smaller than the experimental value of Le Roy *et al.* The finite-mass calculation with the relativistic correction is closer to experiment than the infinite-mass C_3, but there is a remaining discrepancy of 0.0017 a.u. It is not likely that QED effects can explain the discrepancy, as Pachucki *et al.* found that these were 2.5 times smaller than relativistic effects in the polarizability of helium [41]. It must be recalled that the Le Roy *et al.* experiment is reporting an order-of-magnitude improvement in experimental precision. Going to such extreme levels of precision means there might be small corrections that need to be applied to the analysis of the data that have not received consideration. For example, the value of C_3 will be different for states asymptotic to the $2\,^2P_{1/2}$ and $2\,^2P_{3/2}$ levels. The analysis of Le Roy *et al.* uses a common C_3 value for both members of the spin-orbit doublet. Irrespective of this, it should be noted that experiment and theory are incompatible at precisions better than 0.01%.

The difference between the present value of C_3 and that of Le Roy *et al.* is used to assign an error to the present polarizability calculation. Changes of 0.008% were made to the $2(3)^2S$–$2(3)^2P$ matrix elements, the polarizabilities were recomputed, and the differences assigned as the uncertainty in the recommended values. This difference is actually larger than the estimated relativistic change in the matrix element. Therefore, the recommended static polarizability of the Li ground state is 164.11(3) a.u. Uncertainties in the $2(3)^2P$–$3\,^2D$ matrix elements are smaller (relativistic effects have a smaller impact on these matrix elements) and have not been included in the uncertainty analysis. The final value for the static scalar polarizability of the $2\,^2P$ state was 126.970(4) a.u., while the tensor polarizability was 1.612(4) a.u.

The same uncertainty analysis was applied to the Be$^+$ ion polarizabilities. The recommended value for the ground state is 24.489(4) a.u. The static $2\,^2P$ scalar polarizability was set as 2.0285(10) a.u. while the tensor polarizability was set to 5.8528(10) a.u.

Uncertainties in the recommended dynamic polarizabilities in Tables II–V were computed by making corrections to the matrix elements, recomputing, and then observing the change. These uncertainties are best interpreted as indicative, as opposed to rigorous estimates.

VI. SUMMARY

Definitive nonrelativistic values for the dynamic dipole polarizabilities of Li and Be$^+$ in their low-lying $2\,^2S$ and $2\,^2P$ states have been established using the variational method with Hylleraas basis sets. Calculation for both finite and infinite nuclear-mass systems have been performed. Analytic

representations for the dynamic polarizabilities of the Li atom and the Be$^+$ ion have also been developed. These results can serve as a standard against which any other calculation can be judged.

Subsidiary calculations have been used to estimate the impact of relativistic effects that are not explicitly included in the Hylleraas calculation. It is recommended that the value of 164.11(3) a.u. be adopted as the static polarizability of ^{7}Li. The uncertainty of 0.03 a.u. is based on the difference between the present C_3 and that of Le Roy *et al.* [8]. This accuracy level is also supported by the ^{7}Li $2\,^2S$–$2\,^2P_{1/2}$ Stark shift of -37.14 a.u., which is in perfect agreement with the value of $-37.14(2)$ given by the high precision experiment of Hunter *et al.* [13]. The recommended static polarizability for Be$^+$ is 24.489(4) a.u.

The dynamic polarizabilities that have been obtained can be used as an atom-based standard for electromagnetic field intensity. These polarizabilities can be regarded as an initial attempt to develop atom-based standards for polarizability and Stark-shift measurements. The primary virtue of the method with which the relativistic corrections were evaluated was simplicity of computation. For present purposes, the estimate of the relativistic corrections only has to be accurate to 10%–20% for the recommended polarizabilities to be valid. The comparisons that have been done with fully relativistic calculations suggest that the estimates of the relativistic corrections are indeed accurate at this level. However, a more rigorous estimate using the Briet-Pauli Hamiltonian and perturbation theory would be desirable [41–43].

[1] T. Rosenband, D. B. Hume, P. O. Schmidt, C. W. Chou, A. Brusch, L. Lorini, W. H. Oskay, R. E. Drullinger, T. M. Fortier, J. E. Stalnaker, S. A. Diddams, W. C. Swann, N. R. Newbury, W. M. Itano, D. J. Wineland, and J. C. Bergquist, Science **319**, 1808 (2008).

[2] H. S. Margolis, G. P. Barwood, G. Huang, H. A. Klein, S. N. Lea, K. Szymaniec, and P. Gill, Science **306**, 1355 (2004).

[3] M. Chwalla, J. Benhelm, K. Kim, G. Kirchmair, T. Monz, M. Riebe, P. Schindler, A. S. Villar, W. Hänsel, C. F. Roos, R. Blatt, M. Abgrall, G. Santarelli, G. D. Rovera, and Ph. Laurent, Phys. Rev. Lett. **102**, 023002 (2009).

[4] Z. W. Barber, J. E. Stalnaker, N. D. Lemke, N. Poli, C. W. Oates, T. M. Fortier, S. A. Diddams, L. Hollberg, C. W. Hoyt, A. V. Taichenachev, and V. I. Yudin, Phys. Rev. Lett. **100**, 103002 (2008).

[5] H. Katori, M. Takamoto, V. G. Pal'chikov, and V. D. Ovsiannikov, Phys. Rev. Lett. **91**, 173005 (2003).

[6] C. A. Stan, M. W. Zwierlein, C. H. Schunck, S. M. F. Raupach, and W. Ketterle, Phys. Rev. Lett. **93**, 143001 (2004).

[7] S. Inouye, J. Goldwin, M. L. Olsen, C. Ticknor, J. L. Bohn, and D. S. Jin, Phys. Rev. Lett. **93**, 183201 (2004).

[8] R. J. Le Roy, N. S. Dattani, J. A. Coxon, A. J. Ross, P. Crozet, and C. Linton, J. Chem. Phys. **131**, 204309 (2009).

[9] A. Miffre, M. Jacquey, M. Büchner, G. Trénec, and J. Vigué, Phys. Rev. A **73**, 011603(R) (2006).

[10] C. R. Ekstrom, J. Schmiedmayer, M. S. Chapman, T. D. Hammond, and D. E. Pritchard, Phys. Rev. A **51**, 3883 (1995).

[11] A. D. Cronin, J. Schmiedmayer, and D. E. Pritchard, Rev. Mod. Phys. **81**, 1051 (2009).

[12] K. E. Miller, D. Krause, and L. R. Hunter, Phys. Rev. A **49**, 5128 (1994).

[13] L. R. Hunter, D. Krause, D. J. Berkeland, and M. G. Boshier, Phys. Rev. A **44**, 6140 (1991).

[14] L. R. Hunter, D. Krause, K. E. Miller, D. J. Berleland, and M. G. Boshier, Opt. Commun. **94**, 210 (1992).

[15] R. Ashby, J. J. Clarke, and W. A. van Wijngaarden, Eur. Phys. J. D **23**, 327 (2003).

[16] G. D. Stevens, C.-H. Iu, T. Bergeman, H. J. Metcalf, I. Seipp, K. T. Taylor, and D. Delande, Phys. Rev. Lett. **75**, 3402 (1995).

[17] L. Y. Tang, Z. C. Yan, T. Y. Shi, and J. F. Babb, Phys. Rev. A **79**, 062712 (2009).

[18] Z.-C. Yan, J. Y. Zhang, and Y. Li, Phys. Rev. A **67**, 062504 (2003).

[19] Z. C. Yan, J. F. Babb, A. Dalgarno, and G. W. F. Drake, Phys. Rev. A **54**, 2824 (1996).

[20] S. Cohen and S. I. Themelis, J. Chem. Phys. **124**, 134106 (2006).

[21] J. Y. Zhang, J. Mitroy, and M. W. J. Bromley, Phys. Rev. A **75**, 042509 (2007).

[22] W. R. Johnson, U. I. Safronova, A. Derevianko, and M. S. Safronova, Phys. Rev. A **77**, 022510 (2008).

[23] L. Y. Tang, J. Y. Zhang, Z. C. Yan, T. Y. Shi, J. F. Babb, and J. Mitroy, Phys. Rev. A **80**, 042511 (2009).

[24] D. K. McKenzie and G. W. F. Drake, Phys. Rev. A **44**, R6973 (1991).

[25] Z. C. Yan and G. W. F. Drake, J. Phys. B. **30**, 4723 (1997).

[26] M. Mérawa, M. Rérat, and C. Pouchan, Phys. Rev. A **49**, 2493 (1994).

[27] A. Derevianko, S. G. Porsev, and James F. Babb, At. Data Nucl. Data Tables **96**, 323 (2010).

[28] M. Mérawa and M. Rérat, J. Chem. Phys. **108**, 7060 (1998).

[29] J. Pipin and D. M. Bishop, Phys. Rev. A **45**, 2736 (1992).

[30] V. E. Chernov, D. L. Dorofeev, I. Yu. Kretinin, and B. A. Zon, Phys. Rev. A **71**, 022505 (2005).

[31] T. Kobayashi, K. Sasagane, and K. Yamaguchi, Int. Quantum Chem. **65**, 665 (1997).

[32] J. Muszynska, D. Papierowska, J. Pipin, and W. Woznicki, Int. Quantum Chem. **22**, 1153 (1982).

[33] M. S. Safronova, B. Arora, and C. W. Clark, Phys. Rev. A **73**, 022505 (2006).

[34] Y. Ralchenko, A. E. Kramida, J. Reader, and NIST ASD Team (2008). NIST Atomic Spectra Database (version 3.1.5), [Online]. Available at http://physics.nist.gov/asd3 [2009, September 17]. National Institute of Standards and Technology, Gaithersburg, MD.

[35] G. W. F. Drake, *Handbook of Atomic, Molecular, and Optical Physics* (American Institute of Physics, New York, 1996).

[36] J. Y. Zhang and Z. C. Yan, J. Phys. B **37**, 723 (2004).

[37] J. Mitroy and M. W. J. Bromley, Phys. Rev. A **68**, 052714 (2003).

[38] I. S. Lim, M. Pernpointner, M. Seth, J. K. Laerdahl, P. Schwerdtfeger, P. Neogrady, and M. Urban, Phys. Rev. A **60**, 2822 (1999).

[39] W. I. McAlexander, E. R. I. Abraham, and R. G. Hulet, Phys. Rev. A **54**, R5 (1996).

[40] J. Mitroy and M. S. Safronova, Phys. Rev. A **79**, 012513 (2009).

[41] K. Pachucki and J. Sapirstein, Phys. Rev. A **63**, 012504 (2000).

[42] W. Cencek, K. Szalewicz, and B. Jeziorski, Phys. Rev. Lett. **86**, 5675 (2001).

[43] G. Lach, B. Jeziorski, and K. Szalewicz, Phys. Rev. Lett. **92**, 233001 (2004).